INTERNATIONAL JOURNAL FOR NUMERICAL METHODS IN FLUIDS
Int. J. Numer. Meth. Fluids **30**: 105–121 (1999)

A FINITE ELEMENT METHOD FOR TWO-DIMENSIONAL WATER-WAVE PROBLEMS

J.W. KIM* AND K.J. BAI[1]

Department of Naval Architecture and Offshore Engineering, University of California, Berkeley, CA, USA

SUMMARY

In this paper, the authors treat the free-surface waves generated by a moving disturbance with a constant speed in water of finite and constant depth. Specifically, the case when the disturbance is moving with the critical speed is investigated. The water is assumed inviscid and its motion irrotational. The surface tension is neglected. It is well-known that the linear theory breaks down when a disturbance is moving with the critical speed. As a remedy to overcome the invalid linear theory, approximate non-linear theories have been applied with success in the past, i.e. Boussinesq and Korteweg de Vries equations, for example. In the present paper, the authors describe a finite element method applied to the non-linear water-wave problems in two dimensions. The present numerical method solves the exact non-linear formulation in the scope of potential theory without any additional assumptions on the magnitude of the disturbances. The present numerical results are compared with those obtained by other approximate non-linear theories. Also presented are the discussions on the validity of the existing approximate theories applied to two types of the disturbances, i.e. the bottom bump and the pressure patch on the free-surface at the critical speed. Copyright © 1999 John Wiley & Sons, Ltd.

KEY WORDS: non-linear free-surface waves; finite element method; Hamilton's principle; soliton

1. INTRODUCTION

The hydrodynamic problem of water-waves in the offshore regions has been of interest to many naval architects and ocean engineers for a long time. The generation and evolution of the water-waves and their interaction with the manmade structures are the main concerns in this problem. The theoretical investigations on the topic have been usually made in the scope of the potential theory by assuming the effect of viscosity being negligibly small. The most distinctive feature of this problem is the presence of the free-surface as a free-boundary, which should be obtained as a part of solution. Due to this complexity, the theoretical investigation on the problem has been restricted mainly to simplified theories, such as the linear gravity wave theory and the shallow water theory. In the linear gravity wave theory, the non-linearity of the waves is neglected but the effect of dispersion is fully taken into account. On the other hand, in the shallow water theory, the leading order terms of non-linearity are included while the dispersion term is neglected, as in the hydraulics, or considered partially, as in the Korteweg de Vries (KdV) and the Boussinesq theories. Since both the dispersion and the

* Correspondence to: Department of Ocean Engineering, University of Hawaii, 2540 Dole Street, Holmes Hall 402, Honolulu, HI 96822-2303, USA.
[1] Permanent address: Department of Naval Architecture and Ocean Engineering, Seoul National University, Seoul, Republic of Korea.

CCC 0271–2091/99/090105–17$17.50

Received 27 December 1996
Revised 14 May 1998

non-linear effects are known to be comparatively important for the waves in the offshore region, the KdV and the Boussinesq theory are considered as acceptable and useful approximate theories. In general, these theories can predict qualitative features of the wave phenomena in the shallow water region if the amplitude of the waves are not too large. However, in the quantitative comparisons, these results show some deviations from the experiments, especially when the wave amplitude becomes large. To improve the accuracy, one may take into account the higher-order terms neglected in the derivation of the approximate theories. However, it is not easy to treat the higher-order theories for practical applications. Another drawback of these approximate theories is that one cannot determine *a priori* the valid range of these theories before the comparisons are made with the experiments or the exact solutions. Therefore, it seems to be highly desirable to develop an accurate numerical scheme for the exact theoretical model for the validation of the existing approximate theories, as well as for a better prediction for a more realistic physical model.

In this paper, the authors present a numerical method that can be a candidate for these purposes. The present numerical method is a finite element approximation based on the Hamilton principle. The Hamilton principle is given in the case of a fixed fluid domain by Serrin [1]. More general forms of the variational principles for free-surface flow problems are given in [2–4]. The Hamilton principle [1] has been extended for the free-surface flow problems and the finite element method based on the principle has been applied to water-wave problems [5–7].

In the procedure of solving the variational problem, the velocity fields are approximated by finite element basis functions. From the known distinctive characteristics of the velocity field in the depthwise and in the horizontal direction, the authors use the p-version and the h-version finite element discretization for the vertical and the horizontal directions respectively. It is of interest to note that they could obtain the same result of the Green–Naghdi theory when the velocity field is approximated by a depthwise linear streamfunction [6,9].

As an application of the present numerical method, the authors treated wave generation due to a disturbance moving with the critical speed. The convergence of the numerical solution with the increasing order of interpolation is discussed. The present results are compared with those of the Boussinesq and KdV theories. The present results show the validity of the results obtained by the approximate theories.

2. VARIATIONAL PRINCIPLES

A free-surface flow of an inviscid and incompressible fluid, disturbed by the motion of a pressure patch or bottom topography, is considered, as shown in Figure 1. The co-ordinate system is chosen such that the z-axis directs against gravity. The free-surface is denoted by $z = \zeta(x, t)$ and the bottom topography by $x = b(x, t)$.

Hereafter, all the physical variables are non-dimensionalized such that the density of the fluid ρ, gravity g, and the mean water depth h can all be regarded as unity.

The velocity field $\mathbf{u}(x, z, t)$ and the wave elevation $\zeta(x, t)$ can be obtained as a solution of an initial/boundary value problem that consists of the Euler equations and the boundary conditions. However, it can be shown that the initial/boundary value problem can be replaced by equivalent variational problems. Here, the Hamilton principle is used, which states that the true velocity field of the fluid makes the time integral of Lagrangian have a stationary value for an arbitrary variation of the velocity field. The Lagrangian is defined as the difference between the kinetic and the potential energy. The variational principle for a fixed fluid domain

is given in [1]. The extension of the principle modified to include the free-surface conditions can be written as [6]:

$$L = \int \mathscr{L}\, \mathrm{d}x, \tag{1}$$

$$\mathscr{L} = \frac{1}{2}\int_b^\zeta \mathbf{u}\cdot\mathbf{u}\, \mathrm{d}z - \frac{1}{2}(\zeta^2 - b^2) - \int_b^\zeta \mathbf{u}\cdot\nabla\phi\, \mathrm{d}z + \bar{\phi}\zeta_t - \underline{\phi} b_t - \bar{p}\zeta, \tag{2}$$

where L and $\mathscr{L}$ are the Lagrangian and its density respectively, and ϕ denotes a Lagrangian multiplier for the kinematic constraint that can be interpreted as a velocity potential. The terms with overbars ($\bar{\ }$) and under bars ($\underline{\ }$) are the terms evaluated at the free-surface and on the bottom respectively. Taking variation of the time integral of the Lagrangian, the following results can be obtained from the variations of $\mathbf{u}$, ϕ and ζ

$$\frac{\delta L}{\delta \mathbf{u}} = 0:\ \mathbf{u} = \nabla\phi, \quad b < z < \zeta, \tag{3}$$

$$\frac{\delta L}{\delta \phi} = 0:\ \nabla\cdot\mathbf{u} = 0, \quad b < z < \zeta, \tag{4}$$

$$\frac{\mathbf{u}\cdot\mathbf{n}}{n_z} = \zeta_t, \quad z = \zeta, \tag{5}$$

$$\frac{\mathbf{u}\cdot\mathbf{n}}{n_z} = -b_t, \quad z = b, \tag{6}$$

$$\frac{\delta L}{\delta \zeta} = 0:\ \phi_t + \frac{1}{2}\nabla\phi\cdot\nabla\phi + \zeta = \bar{p}. \tag{7}$$

From the variation of $\mathbf{u}$ being zero, the irrotational condition of the velocity field, as given in Equation (3) is obtained, which gives the Lagrange multiplier ϕ as the velocity potential. The kinematic constraints, Equations (4)–(6), i.e. the continuity equation and the boundary conditions on the free-surface and the bottom, are obtained from the variation of the Lagrange multiplier ϕ. The variation of the wave elevation being zero leads to the dynamic free-surface

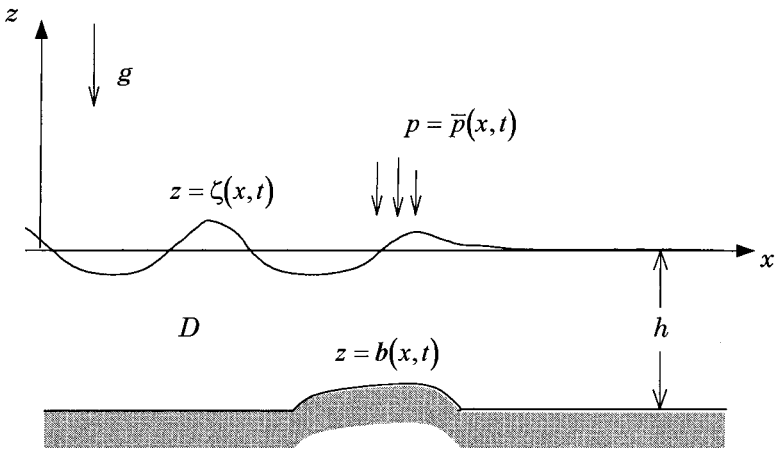

Figure 1. Co-ordinate systems.

condition, Equation (7), i.e. the Bernoulli equation on the free-surface. The Hamilton principle can be written in a more compact form if the irrotational condition or the continuity equation is forced to be satisfied *a priori*. Either of these conditions can be automatically satisfied once the velocity potential or the streamfunction is introduced. The Lagrangian density in velocity potential formulation can be written as

$$\mathbf{u} = \nabla\phi: \ \mathscr{L} = \bar{\phi}\zeta_t - \underline{\phi} b_t - \frac{1}{2}\int_b^\zeta \nabla\phi \cdot \nabla\phi \ \mathrm{d}z - \frac{1}{2}\zeta^2 - \bar{p}\zeta, \tag{8}$$

where the scalar function $\phi(x, z, t)$ is the velocity potential. In the streamfunction formulation, the representation of the velocity field and the Lagrangian can be written as follows:

$$\mathbf{u} = (\psi_z, \ -\psi_x): \ \mathscr{L} = \bar{\phi}(\zeta_t + \bar{\psi}_x) + \frac{1}{2}\int_b^\zeta \nabla\psi \cdot \nabla\psi \ \mathrm{d}z - \frac{1}{2}\zeta^2 - \bar{p}\zeta, \tag{9}$$

where the streamfunction $\psi(x, z, t)$ should satisfy the following kinematic boundary condition on the bottom,

$$\underline{\psi} = -B(x, t) \equiv -\int^x b_t \ \mathrm{d}x, \tag{10}$$

as an essential condition.

3. APPROXIMATION

In the discretization procedure for the variational problem, the velocity fields and the wave elevation are approximated by the finite element basis functions. The most distinct feature of the present problem is the presence of the moving free-surface, which should be obtained as part of a solution. For an efficient discretization of the fluid domain with the moving boundary, the authors adopt a co-ordinate transformation in the z-direction and use the separation of variables. This particular transformation method has a restriction in that the free-surface and the bottom topography should be single-valued functions of horizontal variables. However, the present variational principles can also be applied to a multivalued free-surface, such as breaking wave, with a more general co-ordinate transformation or mesh generation technique.

Since the fluid domain is variable due to the surface elevation $\zeta(x, t)$ and the bottom topography $b(x, t)$, it is more convenient to adopt a transformed co-ordinate system (x, γ), such that

$$\gamma = \frac{z - b}{\theta}, \quad \theta = \zeta - b, \tag{11}$$

$$\phi(x, z, t) = \phi^*(x, \gamma, t), \qquad \psi(x, z, t) = \psi^*(x, \gamma, t).$$

Then the Lagrangian density can be written as

$$\mathscr{L} = \bar{\phi}^*\zeta_t - \underline{\phi}^* b_t - \frac{1}{2}\int_0^1 \left\{\theta\phi_x^{*2} - 2(b_x + \gamma\theta_x)\phi_x^*\phi_\gamma^* + \frac{1}{\theta}\{1 + (b_x + \gamma\theta_x)^2\}\phi_\gamma^{*2}\right\} \mathrm{d}\gamma$$
$$- \frac{1}{2}(\zeta^2 - b^2) - \bar{p}\zeta \tag{12}$$

for the velocity potential formulation and

$$\mathscr{L} = \bar{\phi}(\zeta_t + \bar{\psi}_x) + \frac{1}{2}\int_0^1 \left[\theta\psi_x^{*2} - 2(b_x + \gamma\theta_x)\psi_x^*\psi_\gamma^* + \frac{1}{\theta}\{1 + (b_x + \gamma\theta_x)^2\}\psi_\gamma^{*2}\right] \mathrm{d}\gamma - \frac{1}{2}\zeta^2 - \bar{p}\zeta \tag{13}$$

for the streamfunction formulation. In the transformed co-ordinate system $Ox\gamma$, the computational domain is rectilinear. As a result, separation of variables can be used for the interpolation of the velocity fields. Different interpolation functions are used for the depthwise and the horizontal directions. The discretization procedures for both variational formulations can be written as shown in the next sections.

3.1. Velocity potential formulation

The velocity potential and the wave elevation in the transformed co-ordinate system $Ox\gamma$ are approximated as follows:

$$\phi^*(x, \gamma, t) = \sum_i \sum_{m+1}^{N_p} \phi_{mi}(t) f_m(\gamma) N_i(x), \qquad \zeta(x, t) = \sum_i \zeta_i(t) N_i(x), \tag{14}$$

where $\{f_1(\gamma), f_2(\gamma), f_3(\gamma), \ldots\}$ is the basis function in a Sobolev space, which consists of functions whose derivatives up to first-order are square integrable in $(0, 1)$. Specifically, polynomials will be used for the depthwise interpolation. For the horizontal plane, a piecewise linear basis function is used. For convenience in the treatment of the boundary conditions, the following is set without loss of generality:

$$f_m(1) = \delta_{m1}, \qquad \bar{\phi} = \sum_i \phi_{1i} N_i, \tag{15a}$$

$$f_m(0) = \delta_{m2}, \qquad \underline{\phi} = \sum_i \phi_{2i} N_i. \tag{15b}$$

Substituting the approximate representations, i.e. the assumed representation for the trial functions of the velocity potential and the wave elevation, the Lagrangian can be written as

$$L = \sum_{i,j}\left(M_{ij}\phi_{1i}\frac{\mathrm{d}}{\mathrm{d}t}\zeta_j - \frac{1}{2}M_{ij}\zeta_i\zeta_j\right) - \frac{1}{2}\sum_{m,n,i,j} K_{mnij}\phi_{mi}\phi_{nj} - \sum_i \left\{\left(\int N_i b_t \,\mathrm{d}x\right)\phi_{2i} + \left(\int N_i \bar{p}\,\mathrm{d}x\right)\zeta_i\right\}, \tag{16}$$

where the tensors appearing in the above equations are defined as

$$M_{ij} = \int N_i N_j \,\mathrm{d}x, \tag{17a}$$

$$K_{mnij} = \int\left[A^0_{mn}\theta\frac{\partial N_i}{\partial x}\frac{\partial N_j}{\partial x} - 2b_x B^0_{mn}\frac{\partial N_i}{\partial x}N_j - 2\theta_x B^1_{mn}\frac{\partial N_i}{\partial x}N_j + \frac{1}{\theta}\{(1 + b_x^2)C^0_{mn} + 2b_x\theta_x C^1_{mn} + \theta_x^2 C^2_{mn}\}N_i N_j\right]\mathrm{d}x, \tag{17b}$$

$$A^\alpha_{mn} = \int_0^1 \gamma^\alpha f_m(\gamma) f_n(\gamma)\,\mathrm{d}\gamma, \qquad B^\alpha_{mn} = \int_0^1 \gamma^\alpha f_m(\gamma) f'_n(\gamma)\,\mathrm{d}\gamma, \qquad C^\alpha_{mn} = \int_0^1 \gamma^\alpha f'_m(\gamma) f'_n(\gamma)\,\mathrm{d}\gamma. \tag{17c,d,e}$$

The Euler–Lagrange equation of the above Lagrangian gives the following equations:

$$\sum_j M_{ij} \frac{\mathrm{d}}{\mathrm{d}t} \zeta_j = \sum_{n,j} K^*_{1nij} \phi_{nj}, \tag{18}$$

$$\sum_j M_{ij} \frac{\mathrm{d}}{\mathrm{d}t} \phi_{1j} = -\frac{1}{2} \sum_{m,n,k,l} \frac{\partial K_{mnkl}}{\partial \zeta_i} \phi_{mk} \phi_{nl} - \sum_j M_{ij} \zeta_j - \iint N_i \bar{p} \, \mathrm{d}x \, \mathrm{d}y, \tag{19}$$

$$\sum_{\substack{n,j \\ n \neq 1}} K^*_{mnij} \phi_{nj} = -\sum_j K^*_{m1ij} \phi_{1j} - \delta_{m2} \int N_i b_t \, \mathrm{d}x, \quad m \neq 1, \tag{20}$$

where

$$K^*_{mnij} = \frac{1}{2} (K_{mnij} + K_{nmji}), \tag{21a}$$

$$\begin{aligned} \frac{\partial}{\partial \zeta_k} K_{mnij} = \int \Bigg[& A^0_{mn} N_k \frac{\partial N_i}{\partial x} \frac{\partial N_j}{\partial x} - 2B^1_{mn} \frac{\partial N_k}{\partial x} \frac{\partial N_i}{\partial x} N_j \\ & - \frac{1}{\theta^2} \{(1 + b_x^2) C^0_{mn} + 2 b_x \theta_x C^1_{mn} + \theta_x^2 C^2_{mn}\} N_k N_i N_j \\ & + \frac{2}{\theta} \{b_x C^1_{mn} + \theta_x C^2_{mn}\} \frac{\partial N_k}{\partial x} N_i N_j \Bigg] \mathrm{d}x \end{aligned} \tag{21b}$$

and δ_{ij} denotes the Kronecker delta. Equations (18) and (19) are the evolution equation of the discretized wave elevation and the velocity potential on the free-surface respectively. Equation (20) gives the algebraic relationship between the velocity potential in the fluid domain and that on the free-surface.

3.2. Streamfunction formulation

The Hamilton principle written in terms of the streamfunction can be discretized in a similar way as the velocity potential formulation. The streamfunction and the wave elevation are interpolated as

$$\psi^*(x, y, \gamma, t) = \sum_i \sum_{m=1}^{N_P} \psi_{mi}(t) f_m(\gamma) N_i(x), \tag{22a}$$

$$\zeta(x, t) = \sum_i \zeta_i(t) N_i(x), \tag{22b}$$

$$\bar{\phi}(x, t) = \sum_i \bar{\phi}_i(t) N_i(x), \tag{22c}$$

with the constraint of the bottom boundary condition

$$\psi_{2i}(t) = B(x_i, t), \tag{22.d}$$

where x_i denotes the x co-ordinate of the nodal point of the shape function $N_i(x)$. Then the Lagrangian can be written as

$$L = \sum_{i,j} \left(M_{ij} \bar{\phi}_i \frac{\mathrm{d}}{\mathrm{d}t} \zeta_i + D_{ij} \bar{\phi}_i \psi_{1j} - \frac{1}{2} M_{ij} \zeta_i \zeta_j \right) + \frac{1}{2} \sum_{m,n,i,j} K_{mnij} \psi_{mi} \psi_{nj}, \tag{23}$$

where

$$D_{ij} = \int N_i \frac{\mathrm{d}}{\mathrm{d}x} N_j \, \mathrm{d}x. \tag{24}$$

The Euler–Lagrange equation of the above Lagrangian gives the following equations

$$\sum_j M_{ij} \frac{\mathrm{d}}{\mathrm{d}t} \zeta_j = -\sum_j D_{ij} \psi_{1j}, \tag{25}$$

$$\sum_j M_{ij} \frac{\mathrm{d}}{\mathrm{d}t} \bar{\phi}_j = \frac{1}{2} \sum_{m,n,k,l} \frac{\partial K_{mnkl}}{\partial \zeta_i} \psi_{mk} \psi_{nl} - \sum_j M_{ij} \zeta_j - \int N_i \bar{p} \, \mathrm{d}x, \tag{26}$$

$$\sum_{\substack{n,j \\ n \neq 2}} K^*_{mnij} \psi_{nj} = -\sum_j K^*_{m2ij} \psi_{2j} + \delta_{m1} D_{ji} \bar{\phi}_j, \quad m \neq 2. \tag{27}$$

Equations (25) and (26) are the evolution equation of the discretized wave elevation and the velocity potential on the free-surface respectively. Equation (27) gives the algebraic relationship between the streamfunction in the fluid domain and the velocity potential on the free-surface.

Summarizing this section, obtained after the spatial discretization, was the first-order ordinary differential equations for the surface elevation and the velocity potential on the

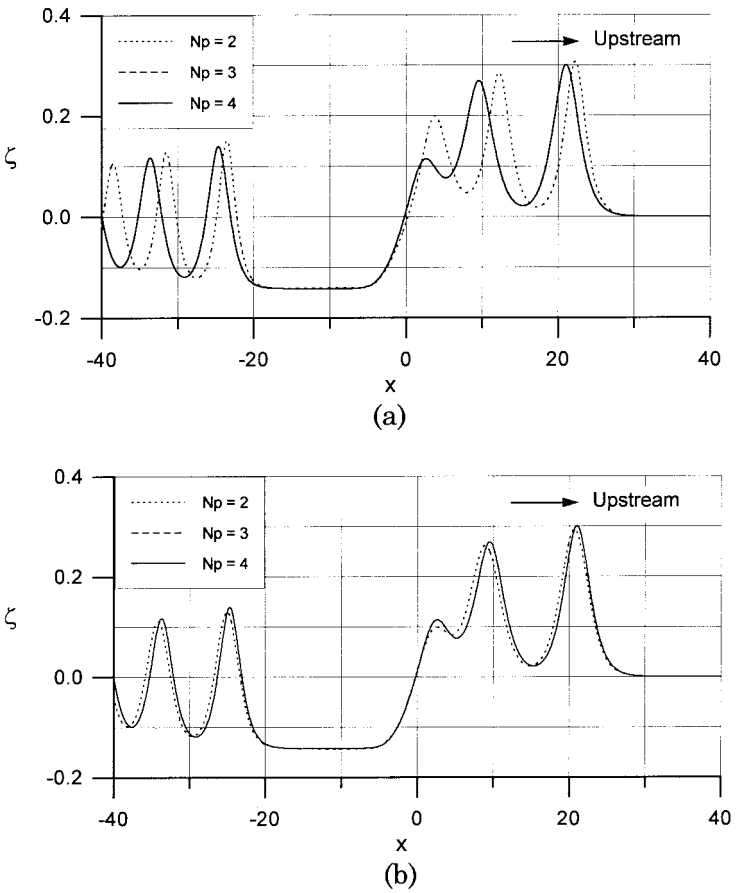

Figure 2. Convergence of numerical solutions for $P_{\max} = 0.03$ at $t = 200$; (a) velocity potential formulation, (b) streamfunction formulation, (c) wave profiles near the leading crest.

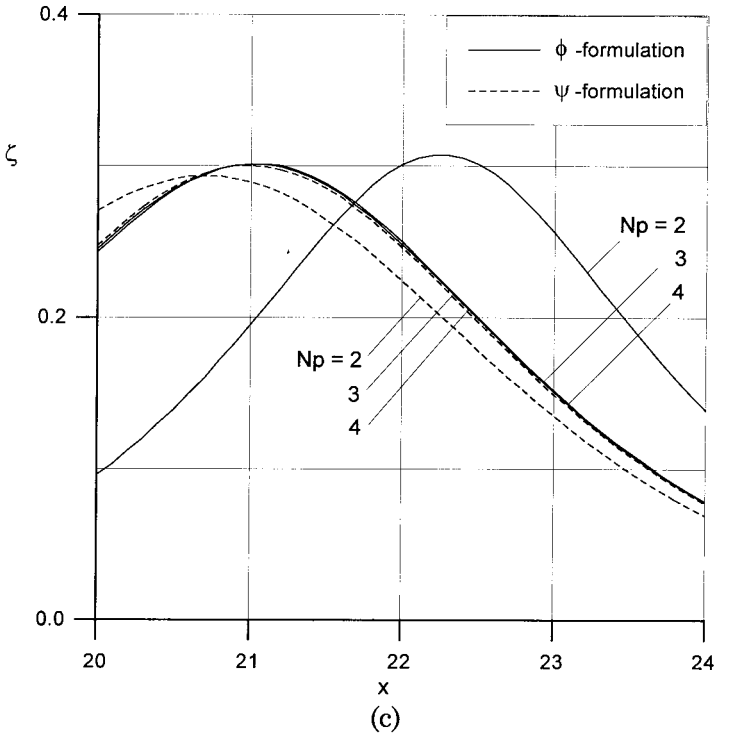

Figure 2 (*Continued*)

free-surface. The variables in the fluid domain are treated as dependent variables of them through the algebraic equations given in Equations (20) and (27). These evolution equations can be integrated numerically to obtain approximate solutions in the time domain.

4. NUMERICAL RESULTS AND DISCUSSIONS

When a ship is moving in a canal near the critical speed $\sqrt{gh}$, it has been known that the flow cannot reach the steady state. The continual generation of solitons at the upstream of the disturbances have been observed in the experiments of Ertekin *et al.* [8] for three-dimensional flow in a canal. Lee *et al.* [10] observed the same phenomenon in their experiments for two-dimensional flow. The theoretical study on this problem has been usually made by using the shallow water approximations, such as the generalized Boussinesq (gB) and forced KdV (fKdV) equations, based on the Boussinesq and KdV theory respectively [10,11]. Recently, Cao *et al.* [12] made a full non-linear computation using the boundary integral method. They showed that the fully non-linear solution predicts larger solitons than the fKdV solution when a strong pressure patch is advancing at the critical speed. They also showed that the wave patterns caused by the pressure patch and the bottom bump show significant difference, although they are predicted to be identical in the fKdV equation.

In the present computations, the authors assess the convergence of the present numerical method. Once the numerical solution is converged, the result is regarded as a numerically exact solution and compared with the results from the gB equations and fKdV equation.

The disturbances of the uniformly translating surface pressure and/or bottom bump are given as

$$\bar{p}(x,t)=\begin{cases} P_{\max}\cos^2\left\{\dfrac{\pi}{L}(x-Ut)\right\}, & -\dfrac{L}{2}<x-Ut<\dfrac{L}{2} \\ 0, & \text{otherwise} \end{cases} \tag{28}$$

$$b(x,t)=\begin{cases} -1+B_{\max}\cos^2\left\{\dfrac{\pi}{L}(x-Ut)\right\}, & -\dfrac{L}{2}<x-Ut<\dfrac{L}{2} \\ -1, & \text{otherwise} \end{cases} \tag{29}$$

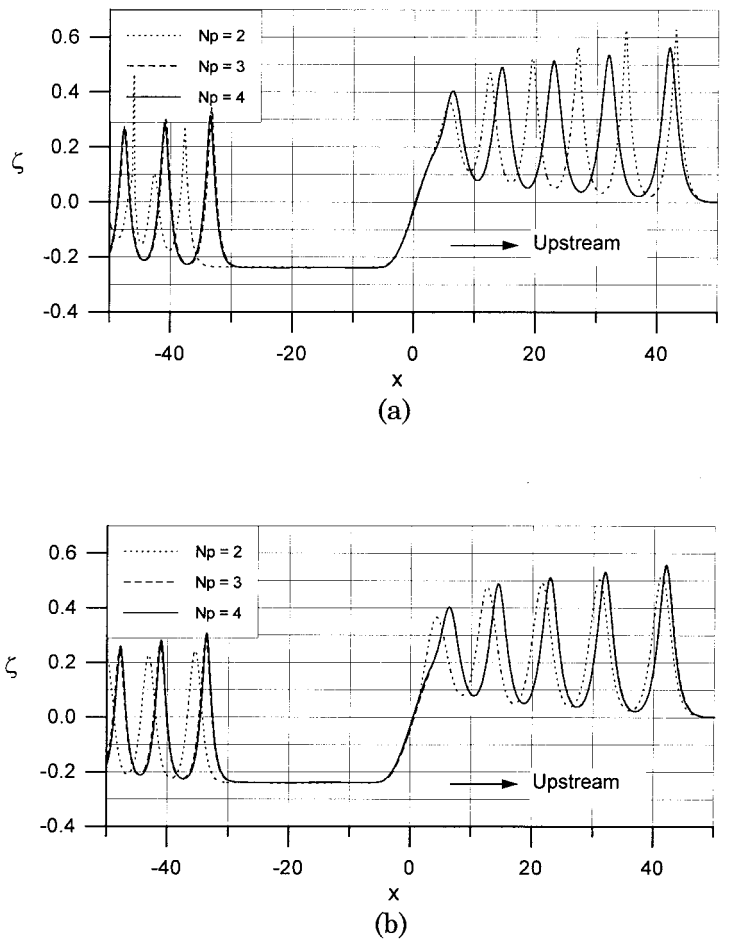

Figure 3. Convergence of numerical solutions for $P_{\max}=0.09$ at $t=200$; (a) velocity potential formulation, (b) streamfunction formulation, (c) wave profiles near the leading crest.

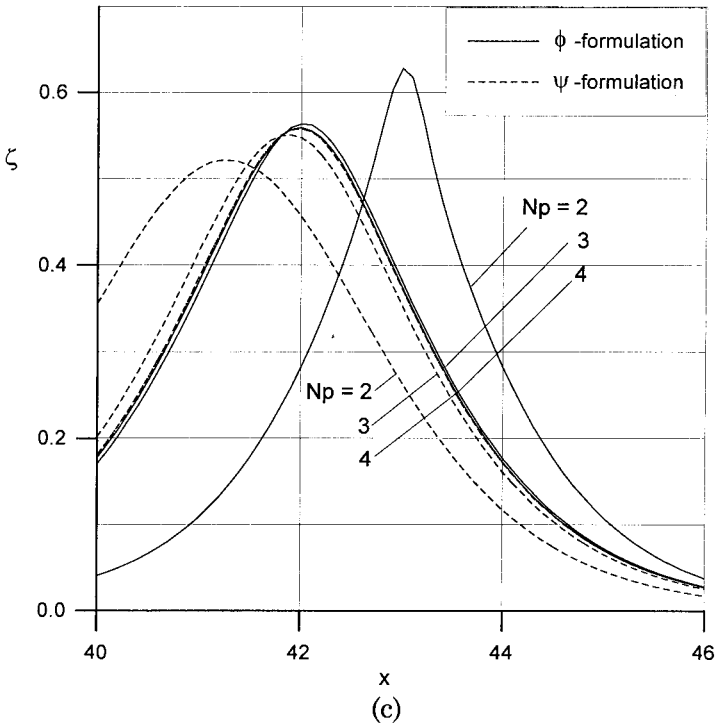

Figure 3 (*Continued*)

Here $P_{\max}$ and $B_{\max}$ denote the maximum magnitude of the pressure patch and the maximum deviation of the bottom bump respectively, and the span of the disturbances L, is taken as $10h$, and the translating speed U is taken as $\sqrt{gh}$, which is the critical speed of the linear gravity wave. The initial conditions are given as

$$\phi(x, z, 0) = 0, \qquad \zeta(x, 0) = -\bar{p}(x, 0). \tag{30}$$

As a depthwise interpolation, polynomials are used. For a given number of interpolation functions, N_p, the polynomials are given as

$$f_1(\gamma) = \gamma, \qquad f_2(\gamma) = 1 - \gamma, \qquad f_3(\gamma) = \gamma(1 - \gamma), \ldots, F_{N_p}(\gamma) = \gamma^{N_p - 2}(1 - \gamma), \tag{31}$$

which is the basis of polynomials of order $N_p - 1$, which satisfies end conditions given in Equations (15a) and (15b).

In the horizontal direction, a piecewise linear interpolation function is used. The discretized equations are integrated in the time domain by the Runge–Kutta fourth-order method. The horizontal mesh size and the time step are fixed as

$$\Delta x = \Delta t = 0.1. \tag{32}$$

The effect of the further refinement of Δx and Δt was less significant than the refinement of the order of depthwise interpolation. With the fixed resolution of horizontal mesh and time step given in (32), the convergence of the numerical solution is investigated by increasing the order of depthwise interpolation. The numerical solution is taken as converged if the upstream wave elevation does not change more than 10^{-3} after N_p is increased two times. The

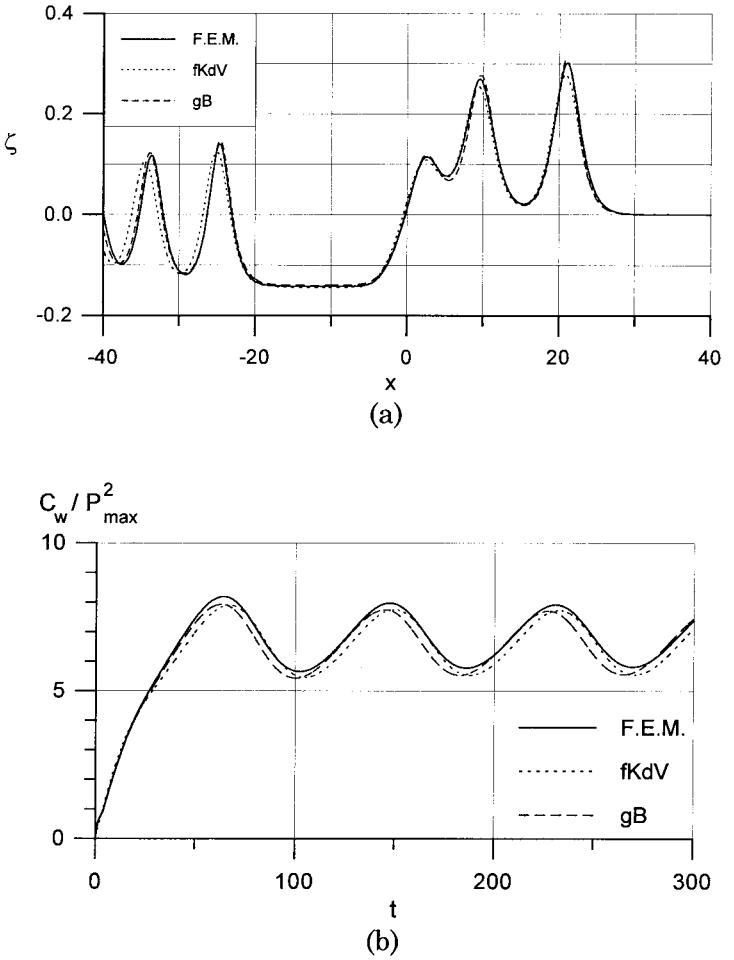

Figure 4. Comparison with approximate theories for $P_{\max} = 0.03$; (a) wave profile at $t = 200$, (b) wave resistance.

converging rate depends on the strength of the disturbances. In Figures 2 and 3, the wave profiles are plotted at $t = 200$ in the case of $P_{\max} = 0.03$ and 0.09, respectively. When $P_{\max} = 0.03$, $N_p = 3$ is sufficient to get a converged solution for both of the velocity potential and the streamfunction formulation. However, when $P_{\max} = 0.09$, $N_p = 4$ is required to obtain a converged solution. The converged wave profiles of the two different formulations agree well each other. The convergence test was also made in the case of a uniform translation of a bottom bump. The rate of convergence was almost same to that of the pressure patch.

Since it has been confirmed that the present scheme gives converged numerical results, the result may be used to validate other approximate theories. For this purpose, numerical computations for the KdV and Boussinesq approximations were carried out following [10,11]. In the comparisons, the present numerical results are obtained by using $N_p = 5$.

In Figures 4 and 5, the results of the pressure patch are shown. The approximate theories show a qualitative agreement with the present finite element approximation. When the forcing is small, the agreement between the finite element and the Boussinesq theory is very good. However, as the forcing becomes large, the Boussinesq theory does not provide any better results than the KdV theory does, as shown in Figure 5.

The results of the bottom bump are shown in Figures 6 and 7. In the case of the bottom bump, the KdV theory shows poor agreement with the finite element compared with the case of the pressure patch. The disagreement of KdV theory increases when the forcing is stronger. However, the Boussinesq theory shows the same tendency of the agreement to the case of pressure patch.

In the overall comparison, the Boussinesq solution agrees well with the present theory, and the KdV solution also shows a good agreement in the case of the pressure patch. It is of interest to note that, in the case of the pressure patch, the numerical results using the KdV equation agree quite well with the present fully non-linear model, even for the strong disturbances, for which the results of Cao *et al.* showed considerable difference between their numerical solution using boundary integral method. The reason may be explained after noting that a lager value for the length of the disturbances ($L = 10h$) than theirs ($L = 2h$) was used. For comparison, a computation using $L = 2h$ and $P_{\max} = 0.1$, which is also treated in Cao *et al.*, was performed. The results are shown in Figure 8. The shallow water approximations do not agree well with the fully non-linear models. The agreement between the finite element method and boundary integral method is good. It seems that the length of the disturbance is also an important parameter for the validity of the shallow approximate theories, since the

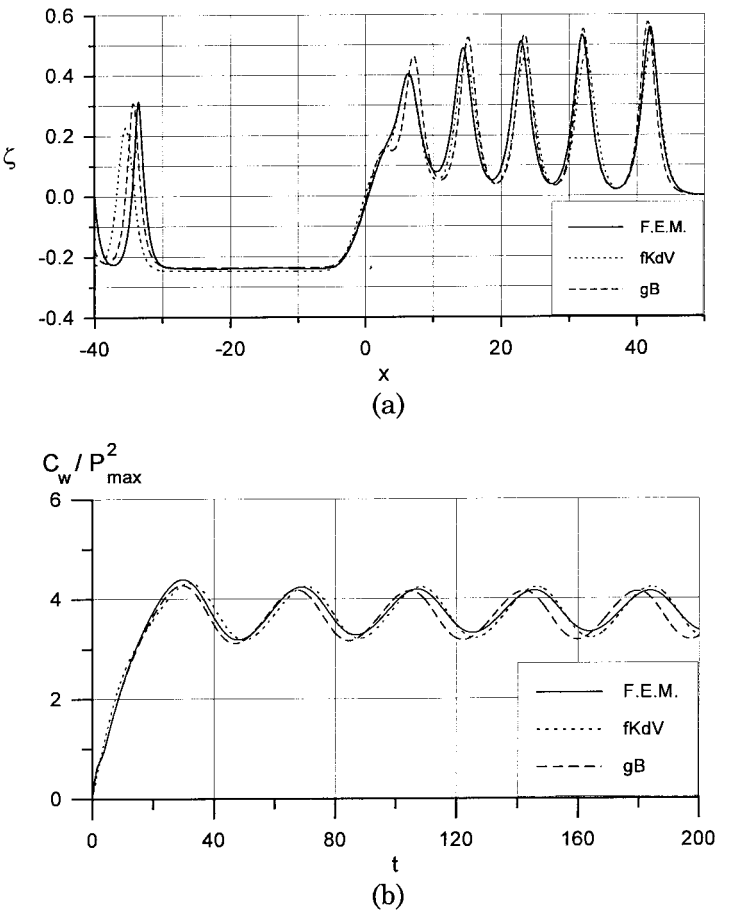

Figure 5. Comparisons with approximate theories for $P_{\max} = 0.09$; (a) wave profile at $t = 200$, (b) wave resistance.

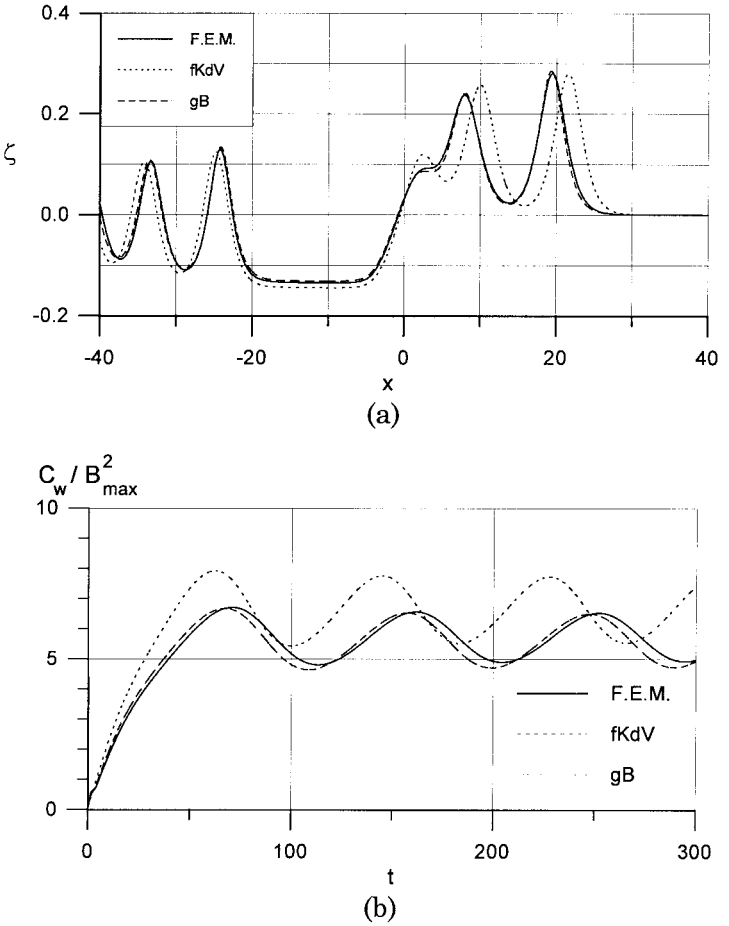

Figure 6. Comparisons with approximate theories for $B_{\max} = 0.03$; (a) wave profile at $t = 200$, (b) wave resistance.

length of the disturbance is also assumed to be long in the derivation of the shallow water theories [11].

More general comparisons are shown in Figure 9, where the mean wave resistance, defined by time-averaged wave resistance between the second and the third peaks, are compared. Unlike the linear theory, the wave resistance is no longer a second-order quantity. The linear regression analysis showed that the mean wave resistance is roughly proportional to 1.5th of the power of the disturbance. In Figure 10, the mean wave resistance is plotted after normalized by 1.5th of the power of the disturbance. The wave resistance of the pressure patch and the bottom bump approach each other as the magnitude of disturbances goes tends to zero. In the KdV theory, the pressure patch and the bottom bump are treated as the equivalent disturbance to the free-surface flow. That assumption seems to be valid only when the disturbance is very small, as shown in Figure 10. However, for the magnitude of disturbance greater than 0.01, which can be regarded as quite small for a practical application, the difference in wave resistance is greater than 10%. It may be concluded that the pressure patch and the bottom bump can be treated as the same only when the magnitude is extremely small. In Figure 11, the wave profiles due to the pressure patch and the bottom bump of the same

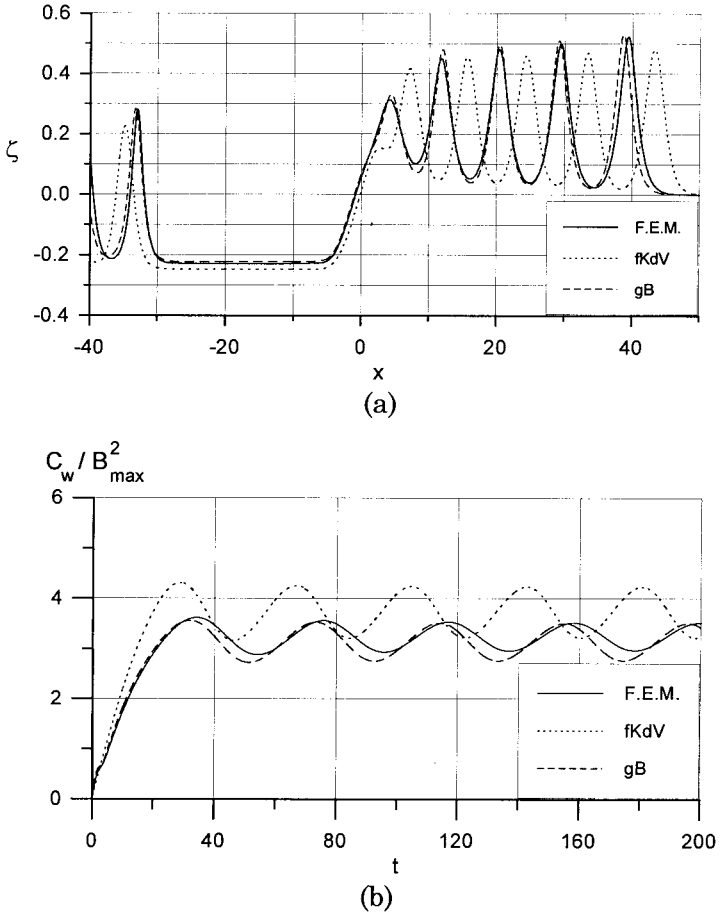

Figure 7. Comparisons with approximate theories for $B_{\max} = 0.09$; (a) wave profile at $t = 200$, (b) wave resistance.

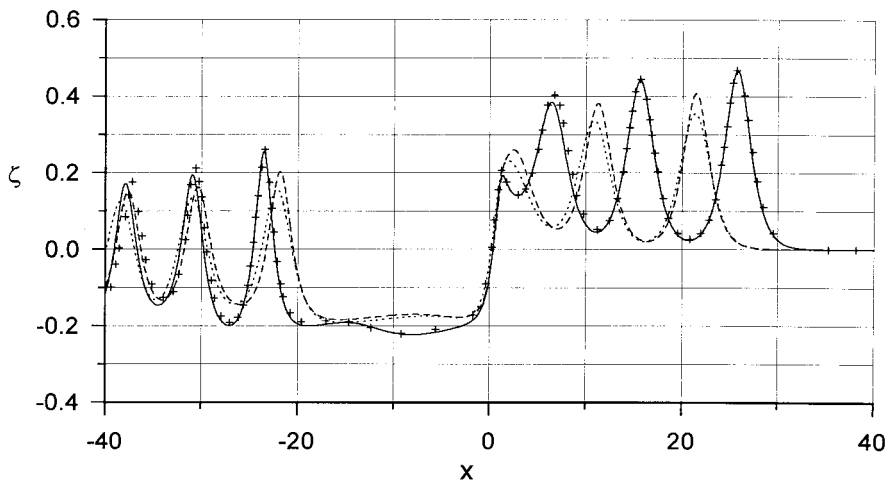

Figure 8. Wave profiles for $L = 2$ and $P_{\max} = 0.1$ at $t = 160$: —, FEM; ---, gB; · · ·, fKdV; + + +, BIM (Cao *et al.* [12]).

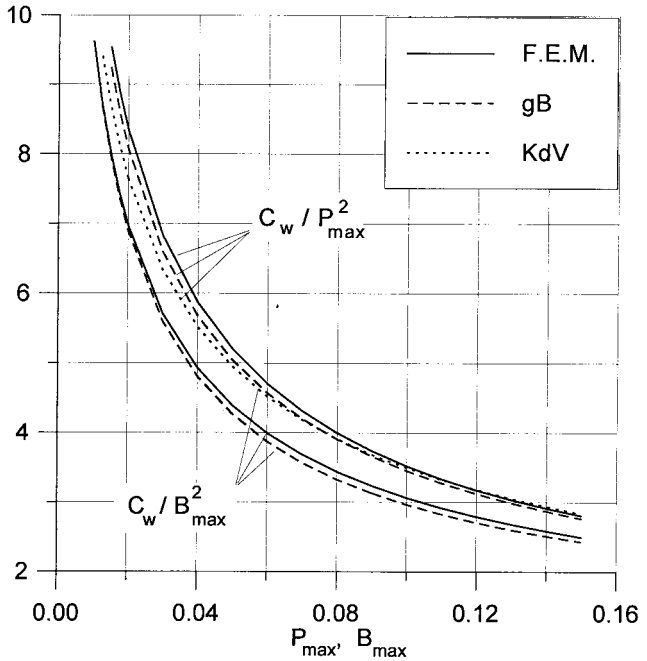

Figure 9. Mean wave resistance coefficient.

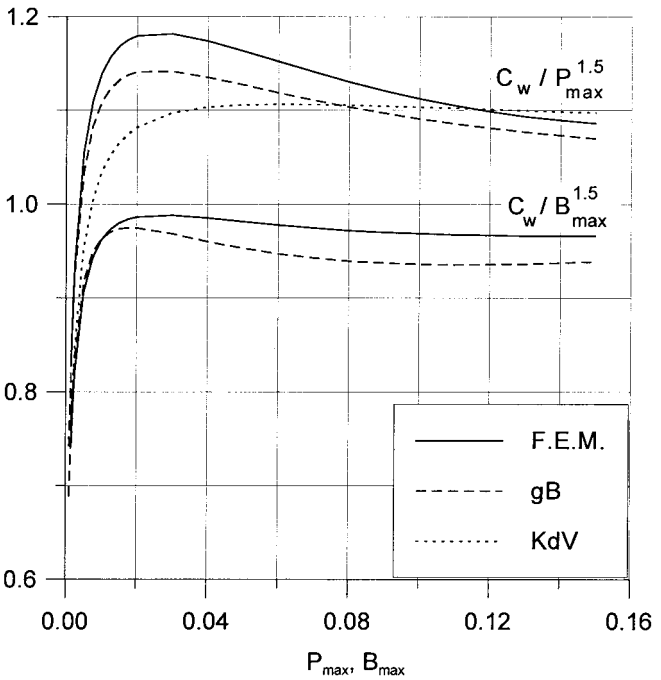

Figure 10. Mean wave resistance coefficient normalized by 1.5th of the power of disturbances.

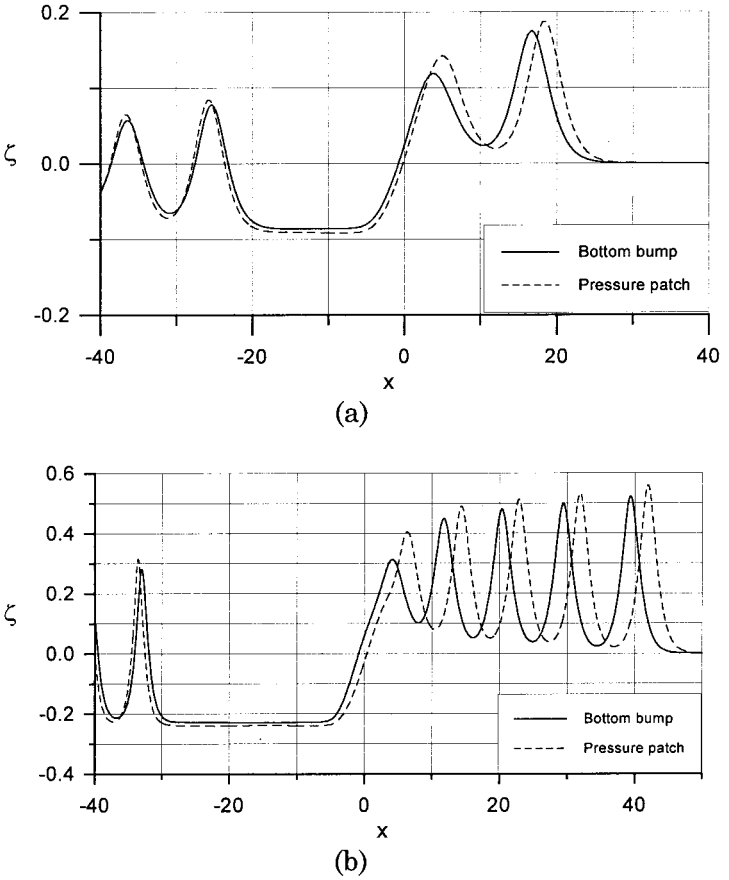

Figure 11. Comparison of the wave profiles generated by the pressure patch and the bottom bump; (a) $P_{\max}$ (or $B_{\max}$) $= 0.0125$, $t = 300$, (b) $P_{\max}$ (or $B_{\max}$) $= 0.09$, $t = 200$.

shape are compared. The figure shows that the pressure patch generates higher waves than the bottom bump. The trend becomes more significant as the amplitude of the disturbances increases.

From these comparisons, it may be concluded that the approximate shallow water theories provide reasonable results to the wave resistance problem at the critical speed. However, for the case of bottom bump, the KdV theory gives a less accurate result. Also, the present numerical method provides accurate results and, therefore, it can be used to examine the validity of the approximate theories and other numerical methods in the future.

ACKNOWLEDGMENTS

The authors are grateful to the Korea Research Foundation and the Korea Science and Engineering Foundation, for partial financial support during the present research.

REFERENCES

1. J. Serrin, 'Mathematical principles of classical fluid mechanics', *Encyclopedia of Physics*, vol. VIII/1, Springer, Berlin, 1958.
2. J.C. Luke, 'A variational principle for a fluid with a free-surface', *J. Fluid Mech.*, **27**, 395–397 (1967).
3. L.J.F. Broer, 'On the Hamiltonian theory of surface waves', *Appl. Sci. Res.*, **30**, 430–446 (1974).
4. J.W. Miles, 'On Hamilton's principle for surface waves', *J. Fluid Mech.*, **83**, 153–158 (1977); and Addendum, **85**, 797 (1978).
5. K.J. Bai, J.W. Kim and Y.H. Kim, 'Numerical computations for a non-linear free-surface problem', *Proc. 5th Int. Conf. On Numerical Ship Hydrodynamics*, Hiroshima, Japan, 1989, pp. 403–418.
6. J.W. Kim and K.J. Bai, 'A note on Hamilton's principle for a free-surface flow problem', *J. Soc. Naval Arch. Korea*, **27**, 19–30 (1990) (in Korean).
7. K.J. Bai and J.H. Han, 'A localized finite element method for the non-linear steady waves due to a two-dimensional hydrofoil', *J. Ship Res.*, **38**, 42–51 (1994).
8. R.C. Ertekin, W.C. Webster and J.V. Wehausen, 'Waves caused by a moving disturbance in a shallow channel of finite width', *J. Fluid Mech.*, **169**, 275–292 (1986).
9. J.W. Kim, K.J. Bai, W.C. Webster and R.C. Ertekin, 'A derivation of Green–Naghdi equation for irrotational flows', submitted to *J. Eng. Math.* (1999).
10. S.J. Lee, G.T Yates and T.W. Wu, 'Experiments and analysis of upstream-advancing solitary waves generated by moving disturbances', *J. Fluid Mech.*, **199**, 569–593 (1989).
11. T.Y. Wu, 'Generation of upstream-advancing solitons by moving disturbances', *J. Fluid Mech.*, **184**, 75–99 (1987).
12. Y.C. Cao, R.F. Beck and W.W. Schultz, 'Numerical computations of two-dimensional solitary waves generated by moving disturbances', *Int. J. Numer. Methods Fluids*, **17**, 905–920 (1993).

